Hindawi
Advances in Civil Engineering
Volume 2023, Article ID 4579238, 12 pages
https://doi.org/10.1155/2023/4579238

Research Article

The Influence of Fly Ash Contents on Mechanical Properties and Energy Response of Concrete at a High Strain Rate

Enbing Yi [1,2]

[1]*School of Energy Science and Engineering, Henan Polytechnic University, Jiaozuo 454150, China*
[2]*China Coal Technology Engineering Group Chongqing Research Institute, Chongqing 400037, China*

Correspondence should be addressed to Enbing Yi; yienbing95@163.com

Received 19 October 2022; Revised 11 December 2022; Accepted 19 December 2022; Published 3 January 2023

Academic Editor: Claudio Mazzotti

The dynamic uniaxial impact compression test was carried out by the Hopkinson pressure bar test system to test the dynamic mechanical properties of concrete with different fly ash contents (P = 0, 10%, 20%, 30%, 40%, and 50%) under 0.3 MPa air pressure. The influences of fly ash content variation on the mechanical characteristics, ductility characteristics (which were calculated according to the concrete ductility formula), energy dissipation characteristics, and surface specific energy variation characteristics (which were calculated by converting the fragments into spheres) of concrete were analyzed, respectively, and the influences of fly ash content variation on the fragment distribution and fractal features of concrete were obtained by statistical analysis. In addition, the application of concrete with the change of fly ash contents in rock burst mine was studied. The results showed that the dynamic peak stress, residual stress, ductility characteristics, fragments distribution, fractal dimension, transmitted energy, dissipated energy, and surface specific energy change significantly with the increase of fly ash contents under dynamic uniaxial impact compression. By analyzing the relationship between surface specific energy and concrete fragment distribution, it could be found that the energy dissipated by stress waves in concrete can be estimated by using the particle size distribution of the field fragments.

1. Introduction

With the increase of high in-situ stress productions such as deep mining of coal mines and excavation of tunnels at large buried depth, the hazards of rock burst caused by high in-situ stress increased gradually. High in-situ stress led to excessive elastic energy accumulation in rocks. When it reached the critical value, the elastic energy would mainly release instantaneously in the form of dissipated energy and kinetic energy, thus causing serious accidents to mining production [1, 2]. With the high in-situ stress conditions, concrete was widely used in roadway shotcrete, bolt reinforcement, roadway support, filling, and other aspects because of its own mechanical properties and energy dissipation characteristics [3]. At present, as the main fuel of thermal power generation, coal would produce a huge amount of fly ash in the combustion process. If fly ash was discarded directly into the natural environment, it would cause significant pollution to the environment. However, fly ash as a concrete preparation material could change the performance of traditional concrete [4, 5] on the one hand, and it could also reduce the manufacturing cost of concrete and reduce environmental pollution [6–8] on the other hand. Therefore, it was of great engineering significance to study the mechanical properties and energy response characteristics of fly ash concrete under the high strain rate for the application of fly ash concrete in the environment with rock burst.

At present, a large number of studies on fly ash concrete show that physical and chemical reactions occur in the solidification process of concrete [9], and these reaction effects have an important impact on concrete's corrosion resistance [10, 11], durability [12, 13], strength [14], permeability [15, 16], energy dissipation, and so on. Bouzoubaa et al. [17] found that the use of fly ash increased the bulk density of mixed cement, thereby reducing the porosity of

mixed cement products. The test of concrete in different curing stages showed that the use of fly ash can improve the compressive strength of concrete in all curing stages. Zhang et al. [18] found that the compressive strength and static elastic modulus of concrete decrease with the increase of fly ash content at 28 days, while the deformation of concrete increases with the increase of fly ash replacement under the same stress level. A series of studies showed that the content variation of fly ash was an important factor influencing the physical and mechanical properties of concrete.

Fly ash concrete was widely used because of its economy and high performance. With the application of more and more fly ash concrete on high in-situ stress environment, it could be found that the stress wave in high in-situ stress environment led to the failure of fly ash concrete. In recent years, some scholars have begun to study the dynamic mechanical properties of fly ash concrete [19–23]. Zhang et al. [24] conducted dynamic splitting tests on concrete with fly ash (contents of 0%, 5%, 10%, 15%, 20%, and 30%) and found that the dynamic splitting tensile strength of concrete with water-cement ratio of 0.45 and 0.6 reaches the maximum value when fly ash content is 10%. Tang et al. [25] found that the addition of fly ash can improve the energy absorption of concrete effectively. Xie et al. [26] studied the failure mode, impact toughness, and other characteristics of fly ash concrete in dynamic impact and found that fly ash contents are significantly correlated with the previous characteristics. A large number of studies have shown that fly ash contents have an important influence on the impact load of concrete.

In view of the significant influence of fly ash content variation on the mechanical properties of concrete, conventional tests mainly focused on its durability, permeability, failure, and other directions, but the mechanical characteristics of concrete with different fly ash content variation under the high strain rate, especially the ductility characteristics, energy dissipation, surface specific energy variation, and its application in rock burst mine were studied relatively. Therefore, in this article, through the dynamic impact compression test results of concrete with six different fly ash contents (P = 0, 10%, 20%, 30%, 40%, and 50%) under 0.3 MPa air pressure, the dynamic mechanical characteristics, ductility characteristics, fragment distribution, fractal dimension, energy dissipation characteristics, and the surface specific energy variation with fly ash contents of concrete samples under the high strain rate were analyzed. The application of concrete with different fly ash contents in rock burst mine was given to provide the reference for its application in dynamic engineering.

2. Materials and Methods

2.1. Concrete Sample Materials with Different Fly Ash Contents. The test concrete ingredients were cement, fly ash, river sand, and tap water. The cement was 42.5 grade ordinary Portland cement produced by Zhonglian Cement Factory in Xuzhou City, and its chemical composition is shown in Table 1. The fineness modulus of the sand was 2.8, the apparent density was 2578 kg/m^3, and the mud content was 2.76%.

The components of fly ash are shown in Table 2. The powder of fly ash was grayish-brown, as shown in Figure 1. The size of glass microbeads ranged from 1 μm to 100 μm, most of which were solid and a few were hollow, as shown in Figure 2.

2.2. Preparation of the Sample. The proportions of various ingredients in fly ash concrete are shown in Table 3. The water-binder ratio was a fixed value of 32.23%. The total mass fraction of fly ash contents in fly ash and cement were 0%, 10%, 20%, 30%, 40%, and 50%, respectively.

As shown in Figure 3, the length, width, and height of the sample were all 100mm cubes. At least 3 concrete specimens should be tested in each test group. The concrete sample was made according to the Standard of Test Method for Physical and Mechanical Properties of Concrete (GB/T50081-2019). The specific steps were as follows: (1) Determine the moisture content of sand; (2) Put cement, sand, fly ash, and water into the mixer for mixing according to the ratio in Table 1, and the mixing time was 180~240 s. The order of adding various ingredients was carried out according to the standard; (3) Put the fully mixed mud into the mold and put it on the shaking table until the surface of the mud oozes water slurry; (4) Smooth the surface of the mold and place the mold with mud in the room (room temperature 20 ± 2°C) for curing for 24~48 h and then remove the mold. Water the mold every 8 hours during the curing period; (5) The concrete samples after demolding were placed in the curing room (temperature 20 ± 2°C, humidity ≥95%) for 28 days; (6) Core, cut, and polish the cube samples, which are finally made of 74 × 37 mm (diameter × height) cylinder samples.

2.3. Test Equipment and Methods. This impact load test was performed by using the split Hopkinson pressure bar test system of a university in Hefei. The schematic diagram of the split Hopkinson pressure bar test system is shown in Figure 4. The test system mainly included loading drive system, pressure bar system, energy absorption system, signal acquisition system, and signal processing system.

The pattern is impacted at 0.3 MPa air pressure using the test instrument as shown in Figure 5. The specific test steps were as follows: open the analysis, test system, software, and set contents according to the test requirements; smear a certain amount of petroleum jelly at both end faces of the sample evenly and place the sample between the incident bar and the transmission bar to clamp, and a protective sleeve on the outer layer of the same position. Open the control valve of the gas tank and adjust the pressure value to 0.3 MPa and then press the switch. When the pressure pointer reaches 0.3 MPa, the system will deflate and the impact process will be completed automatically. Finally, we collect the incident, reflected, and transmitted waves through the strain gauges on the incident and transmitted bars with the signal acquisition system.

Figure 6 was the test signal of fly ash concrete under uniaxial impact compression. It showed that the incident, reflected, and transmitted wave all have good rising edges, which can meet the assumption of stress uniformity.

Table 1: Chemical composition of cement.

SiO_2 (%)	Al_2O_3 (%)	Fe_2O_3 (%)	CaO (%)	MgO (%)	Na_2O (%)	K_2O (%)	SO_3 (%)	Burningloss (%)
21.6	4.13	4.57	64.44	1.06	0.11	0.56	1.74	0.76

Table 2: Chemical composition of fly ash.

SiO_2 (%)	Al_2O_3 (%)	Fe_2O_3 (%)	CaO (%)	MgO (%)	Na_2O (%)	K_2O (%)	SO_3 (%)	Burning loss (%)
54.9	25.8	6.9	8.7	1.8	0.3	0.1	0.6	0.2

Figure 1: Fly ash ingredient.

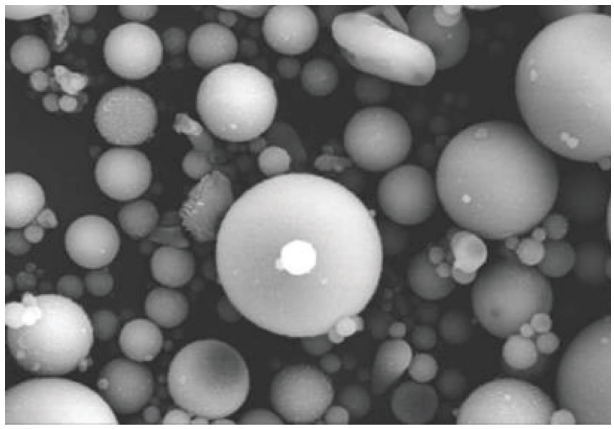

Figure 2: Microstructure of fly ash [25].

3. Mechanical Characteristics of Fly Ash Concrete

3.1. Stress-Strain Curves of Fly Ash Concrete with Different Contents. Figure 7 shows the stress-strain curves of fly ash concrete with different contents. The mechanical properties of concrete with the change of fly ash contents were as follows: (1) the stress-strain curves of concrete with six different fly ash contents experienced the compaction stage, approximate linear elastic stage, softening stage, and crack development stage roughly. (2) With the increase of fly ash content, the strain corresponding to the compaction stage of concrete decreased gradually, and the strain proportion and dynamic peak strain corresponding to the approximate linear elastic stage decreased first and then increased, but the dynamic elastic modulus and peak stress increased first and then decreased. (3) The relative slope of the post-peakstress-strain curve (the absolute value of the slope of the line between peak stress and residual stress) decreased gradually with the increase of fly ash content.

Table 3: The ratio of each material in concrete.

Fly ash contents P (%)	Water-binder ratio (%)	Cement (kg/m^3)	Fly ash (kg/m^3)	Sand (kg/m^3)	Water (kg/m^3)
0	32.23	588.9	0	962	189.8
10	32.23	530.01	58.89	962	189.8
20	32.23	471.12	117.78	962	189.8
30	32.23	412.23	176.67	962	189.8
40	32.23	353.34	235.56	962	189.8
50	32.23	294.45	294.45	962	189.8

3.2. Influence of Fly Ash Contents on Concrete Mechanical Properties

3.2.1. Dynamic Stress Variation Characteristics of Concrete with Different Fly Ash Contents. Figure 8 shows the change curves of concrete dynamic stress and fly ash contents. It can be seen that the change curve mainly includes two stages. In the first stage, when fly ash content rises from 0.00% to 30%, the dynamic peak stress and dynamic residual stress rise, indicating that the rise of fly ash content leads to the gradual increase of concrete impact resistance. In the second stage, with the increase of fly ash content, the dynamic peak stress and dynamic residual stress both decreased when fly ash content rose from 30% to 50%, indicating that the impact resistance of fly ash concrete decreases sharply with the increase of fly ash contents. It was found that the dynamic stress of fly ash concrete is

Figure 3: Fly ash concrete.

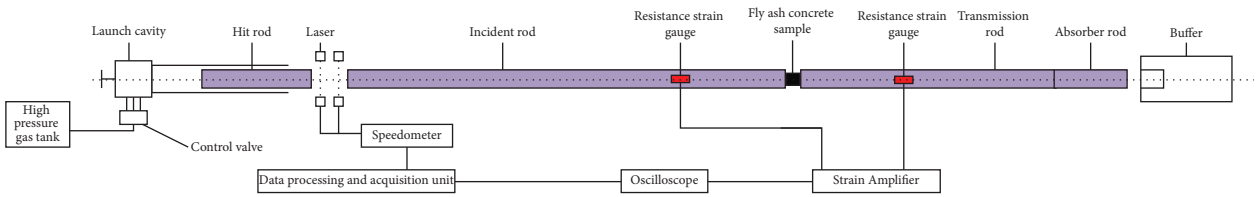

Figure 4: The split Hopkinson pressure bar test system.

Figure 5: Components of the split Hopkinson pressure bar test system.

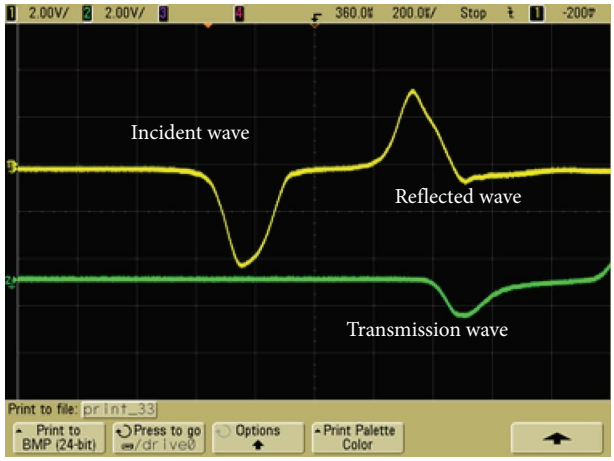

Figure 6: Uniaxial impact compression test signal of fly ash concrete.

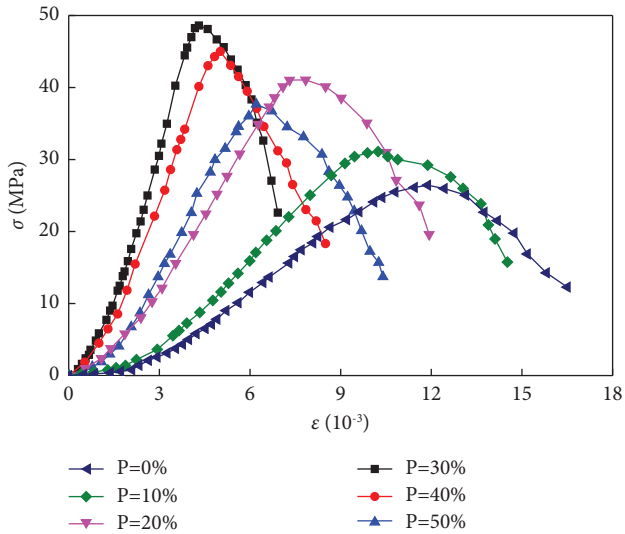

Figure 7: Stress-strain curves of fly ash concrete with different contents.

obviously affected by the change of fly ash contents [27]. In order to better describe the dynamic stress variation with the change of fly ash contents, the peak stress of fly ash concrete and fly ash contents were polynomially fitted as follows (where R^2 represented the correlation coefficient):

$$\begin{cases} \sigma_d = -219.06P^2 + 142.09P + 22.586, & R^2 = 0.9247, \\ \sigma_p = -130.28P^2 + 70.266P + 11.423, & R^2 = 0.91. \end{cases} \quad (1)$$

3.2.2. Dynamic Strain Variation Characteristics of Concrete with Different Fly Ash Contents. Figure 9 shows the change curves of concrete dynamic strain and fly ash contents. It can be seen that the change curve mainly includes two stages. In the first stage, when fly ash content rose from 0.00% to 30%, the dynamic peak strain and dynamic residual strain decreased, indicating that the impact deformation resistance of concrete increases gradually with the increase of fly ash under the high strain rate. In the second stage, with the

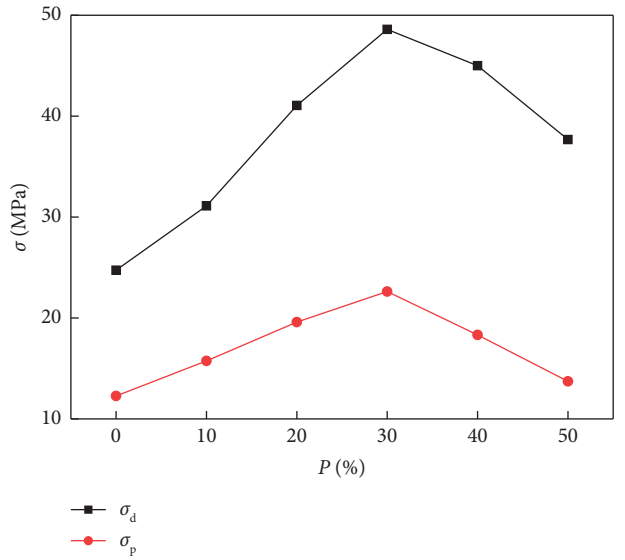

Figure 8: Dynamic stress variation of concrete with the change of fly ash contents.

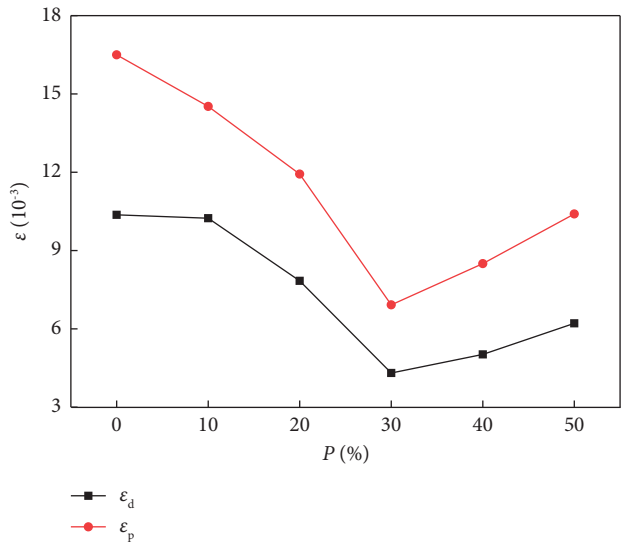

Figure 9: Dynamic strain variation of concrete with the change of fly ash contents.

increase of fly ash content, the dynamic peak strain and dynamic residual strain both rise when fly ash content rises from 30% to 50%, indicating that the impact deformation resistance of fly ash concrete decreases with the increase of fly ash contents. It was found that the dynamic strain of fly ash concrete is affected obviously by the change of fly ash contents. In order to better describe the dynamic strain variation with the change of fly ash contents, the peak strain of fly ash concrete and fly ash contents were polynomially fitted as follows:

$$\begin{cases} \varepsilon_d = 34P^2 - 28.426P + 11.321, & R^2 = 0.8064, \\ \varepsilon_p = 64.249P^2 - 47.52P + 17.436, & R^2 = 0.8627. \end{cases} \quad (2)$$

3.3. Influence of Fly Ash Contents on Concrete Ductility. The stress-strain curve of concrete could reflect the relationship between stress and deformation, and the post-peakstress-strain curve could reflect the influence of fly ash contents on concrete ductility. A large number of studies had shown that the post-peak stress drop can reflect the ductility changes of concrete under different fly ash contents to a certain extent. The expression of the stress drop was as follows [28]:

$$\alpha = \frac{\sigma_d - \sigma_p}{\sigma_d}, \tag{3}$$

where α was the magnitude of stress drop, σ_d was peak stress, and σ_p was the residual stress.

However, it was found that there are limitations to simply using stress drop to express ductility. For example, in the case of the same stress drop, due to the different tendencies of the post-peakstress-strain curve, that is, the different rates of decline of the stress-strain curve in the post-peak stage, the degree of concrete ductility reflected by the curve might not be the same. Therefore, the relative rate of decrease of the stress-strain curve of concrete in the post-peak stage must be considered. The range of the stress drop was at 0–1. In order to make the data more intuitive, we took the logarithm of the relative rate of stress drop and divided it by 10 to keep its range at 0–1. The expression of the relative rate is as follows [28]:

$$\beta = \frac{\lg\left|\sigma_d - \sigma_p/\varepsilon_d - \varepsilon_p\right|}{10}, \tag{4}$$

where β was the relative rate of stress drop, whose geometric significance represented the linear rate at which the peak stress of concrete decreases to the residual stress.

The fly ash concrete was mainly used as a ductility material in engineering. So, the ductility degree of concrete could be expressed with equations (3) and (4) as follows:

$$\lambda = 1 - \alpha\beta = 1 - \frac{\sigma_d - \sigma_p}{\sigma_d} * \frac{\lg\left|\sigma_d - \sigma_p/\varepsilon_d - \varepsilon_p\right|}{10}, \tag{5}$$

where λ was the ductility index. The range of stress drop and its relative rate are both at 0–1, and its product range is also at 0–1 in equation (5). So, the value range of λ should also be at 0–1, and the closer the value of λ is to 0, the weaker the ductility of concrete, and the closer the value of λ is to 1, the stronger the ductility of concrete.

The ductility degree of concrete could be calculated by using equation (5) and combing with the post-peak stage of stress-strain curve of concrete with different fly ash contents.

Figure 10 shows the change curves of concrete ductility and fly ash contents. It can be seen that the higher the fly ash content, the higher the ductility of concrete. When the fly ash content is 0%, the ductility degree is 0.53, which is the maximum value among the fix fly ash contents. With the increase of fly ash content, the ductility degree is 0.38 when the fly ash content is 50%, which is a decrease of 28.55%. By fitting the curve, it is found that the ductility degree increases with the change of fly ash contents, indicating that the increase of fly ash contents leads to the decrease of concrete ductility deformation.

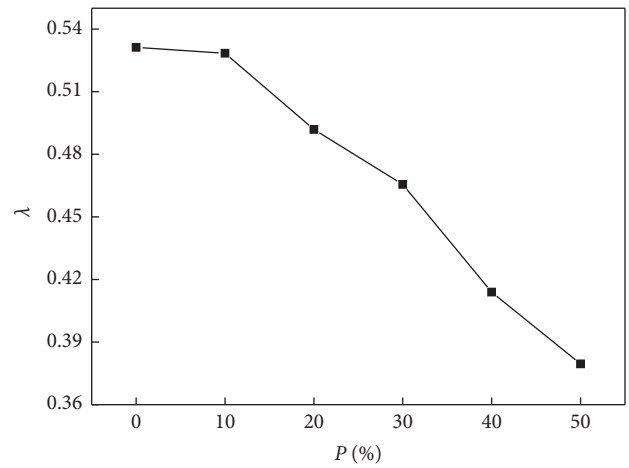

Figure 10: Ductility variation of concrete with the change of fly ash contents.

4. Fragmentation Features of Concrete under Different Fly Ash Contents

4.1. Influence on Fragment Distribution of Concrete with Fly Ash Contents. The fragments of concrete show irregular distribution under the impact load. The fragment distribution of concrete could be obtained by using the mass-size method, and the proportion of fragments under different particle sizes with different fly ash contents was obtained by screening and counting, which could quantify the influence on damage degree of concrete with the variation of fly ash contents. The specific process is as follows: first, the fragments of concrete under different fly ash contents are screened by a graded screen into eight groups of particle sizes: 74–50 mm, 50–30 mm, 30–20 mm, 20–10 mm, 10–5 mm, 5–3 mm, 3–1 mm, and 1–0 mm, and the particle size number i was 1–8, respectively. Then, the mass of each stage of fragments was weighed and recorded with an electronic scale with an accuracy of 0.01 g. At the same time, the percentage of fragment mass in the overall mass of each particle size range n_i is calculated [29]:

$$n_i = m_i/m, \tag{6}$$

where n_i is the mass fraction of fragments at this particle size, m_i is the mass of fragment at this particle size, and m is the overall mass of concrete sample.

We multiply the average particle size r_i of fragments in each grading group and the percentage n_i of fragment mass at this particle size together to get η_i, and we add up the percentage of particle size of fragments at each grading group. The average particle size η of concrete fragments under different fly ash contents [29]:

Table 4: Fragment distribution of concrete with different fly ash contents.

P (%)	74–50 mm	50–30 mm	30–20 mm	20–10 mm	10-5 mm	5-3 mm	3-1 mm	1-0 mm	η
0	0.00	78.23	68.90	48.47	46.07	44.89	51.34	16.47	17.54
10	110.06	84.57	77.03	16.79	18.65	16.77	18.81	14.62	35.37
20	128.44	109.98	74.02	16.71	6.04	4.91	5.27	12.39	40.66
30	139.91	116.70	32.24	28.10	20.87	11.54	6.03	3.45	41.21
40	78.83	89.99	77.52	35.72	13.70	21.09	14.45	18.37	31.99
50	0.00	86.81	65.20	69.38	41.48	34.75	28.98	27.94	18.80

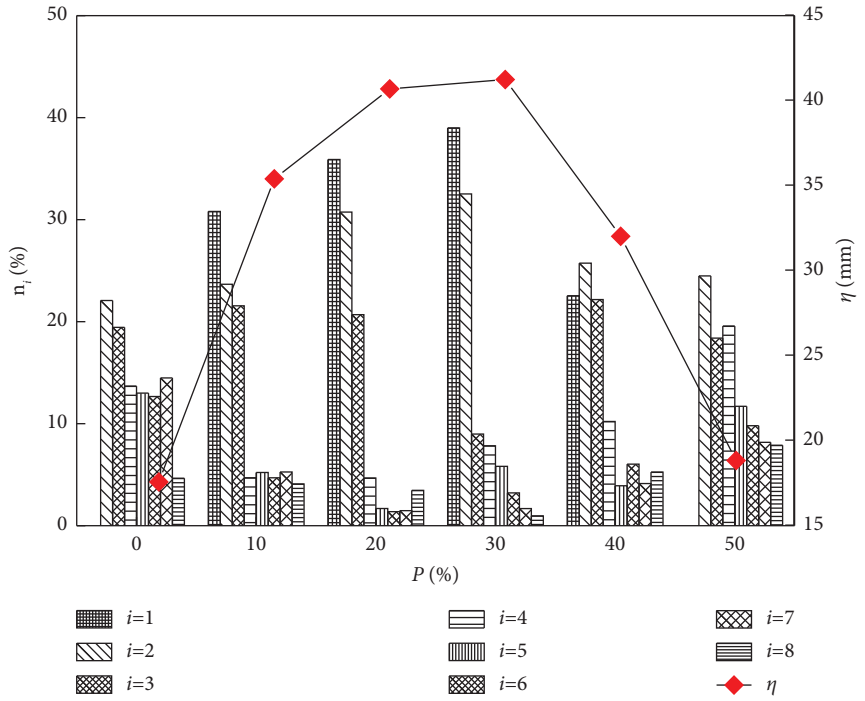

Figure 11: Fragment distribution of concrete with different fly ash contents.

$$\eta = \sum_{i=1}^{8} n_i r_i = \sum_{i=1}^{8} \eta_i, \quad (7)$$

where i is the number of grading screen grades, $i = 1,2, \ldots, 8$ and r_i is the average particle size of fragments screened at each grading group.

Table 4 and Figure 11 show the fragment distribution of concrete with different fly ash contents. It could be seen that the fly ash contents have an important effect on the fragment distribution of concrete. The main performance is as follows: with the increase of fly ash contents, the average particle size increased first and then decreased, and reaching to the maximum of 41.21 mm when the fly ash content is 30%. The mass percentage of fragments with larger particle size (greater than 30 mm) increased first and then decreased, while which with smaller particle size (less than 30 mm) decreased first and then increased.

The results showed that fly ash has a significant impact on the impact resistance of concrete. On the one hand, the addition of fly ash filled part of the gap in the concrete production, making the concrete interior denser, thus enhancing its uniformity. On the other hand, the silicate particles in fly ash such as silicon, iron, and aluminum, underwent secondary hydration reactions with other components of concrete, thus increasing the strength of concrete to a certain extent [30].

4.2. Influence on Fractal Characteristics of Concrete Fragments with Fly Ash Contents. Fractal dimension is widely used in fractal geometry. It can be used to convert the broken and irregular experimental fragments obtained in the experiment process into data so as to describe the breaking law of the experimental samples more accurately. On this basis, the

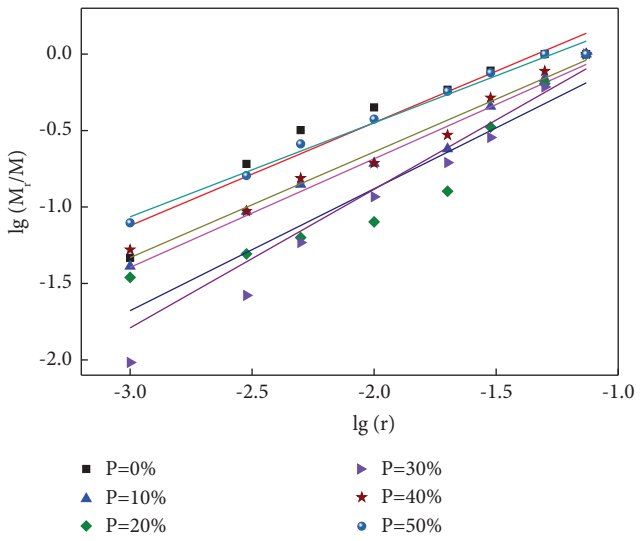

Figure 12: The fractal dimension under the mass-equivalent size.

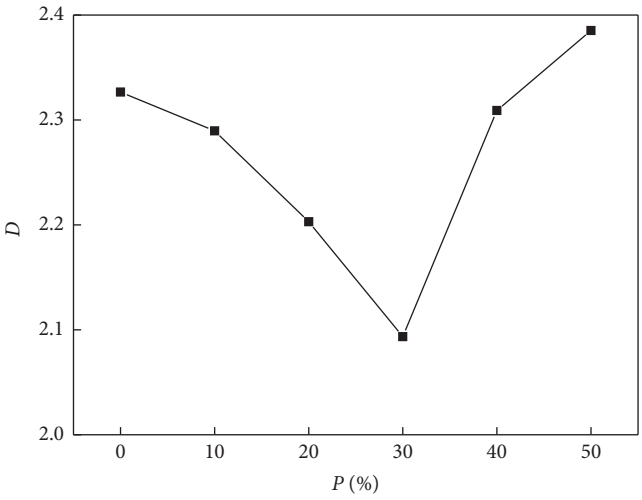

Figure 13: Relationship between the fractal dimension and fly ash contents.

fractal dimension of sandstone fragments is calculated by using the mass-equivalent size [31]:

$$\mathbf{d} = \frac{\lg\left(\mathbf{M_R}/\mathbf{M}\right)}{\lg \mathbf{R}}, \tag{8}$$

$$\mathbf{D} = 3 - \mathbf{d}, \tag{9}$$

where D is the fractal dimension of fragments, d is the slope of a line plotted in double log coordinates, and M_R is cumulative mass of fragments with the diameter less than R.

According to equation (8), the fractal dimension under the mass-equivalent size is calculated as shown in Figure 12. It can be seen that the fractal dimension distribution under the mass-size of sandstone fragments is different under different fly ash contents. The slope of its mass-size increased gradually when the fly ash content increased from 0 to 30% but decreased when the fly ash content increased from 30% to 50%.

Figure 13 shows the fractal dimension of the mass-equivalent size calculated according to equation (9). As shown in Figure 13, the relationship between fractal dimension D and fly ash content P can be divided into two stages. In the first stage, when the fly ash increased from 0.00% to 30%, the fractal dimension decreases, indicating that the damage degree of fly ash concrete is small at this stage, and the addition of fly ash could inhibit the crack propagation of concrete under the high strain rate. With the increase of fly ash content, the fractal dimension increased significantly when the fly ash increased from 30% to 50%, indicating that the damage degree of fly ash concrete increased sharply, and the inhibition effect of fly ash content on the crack propagation of concrete under the high strain rate weakened.

5. Energy Change Law of Concrete under the Change of Fly Ash Contents

5.1. Principle of Concrete Energy Calculation. The failure process of concrete in the Hopkinson impact compression test is a typical energy transformation, which is the process of transforming the kinetic energy carried by the impact bar into the internal energy of the fly ash concrete sample. It would lead to its instability and destruction when the energy inside the fly ash concrete accumulated to a certain extent. The energy carried by the stress wave which was formed by the impact bar hitting the incident bar could be calculated by equation (10) [32, 33]:

$$W = \frac{\mathrm{AC}}{E}\int_0^{\mathbf{t}} \boldsymbol{\sigma}^2(\mathbf{t})\mathbf{dt} = \mathrm{ACE}\int_0^{\mathbf{t}} \boldsymbol{\varepsilon}^2(\mathbf{t})\mathbf{dt}, \tag{10}$$

where A is the cross-sectional area of incident bar and transmission bar, E is the elastic modulus of incident bar and transmission bar, and C is the wave velocity of one-dimensional stress wave. C is related to the density ρ of incident bar and transmission bar and the elastic modulus E, and the relationship between the two could be expressed by equation (11) [32, 33]:

$$\mathrm{C} = \sqrt{E/\rho}. \tag{11}$$

By substituting formulas (10) into (11), the incident energy W_I, reflected energy W_R, and transmitted energy W_P [29, 30] in the dynamic impact process of SHPB could be obtained:

$$\begin{cases} W_I = \mathrm{ACE}\int_0^t \varepsilon_i^2(t)\mathrm{d}t, \\ W_R = \mathrm{ACE}\int_0^t \varepsilon_r^2(t)\mathrm{d}t, \\ W_P = \mathrm{ACE}\int_0^t \varepsilon_t^2(t)\mathrm{d}t, \end{cases} \tag{12}$$

where W_I, W_R, and W_P were the incident, reflected, and transmitted energy, respectively. The dissipation energy W_L

Table 5: Energy distribution of concrete with different fly ash contents.

P (%)	W_R (J)	W_L (J)	W_P (J)
0	30.43	13.35	28.56
10	32.79	16.44	25.36
20	35.42	18.33	19.47
30	38.75	21.91	12.94
40	41.78	15.51	15.28
50	44.36	9.43	18.44

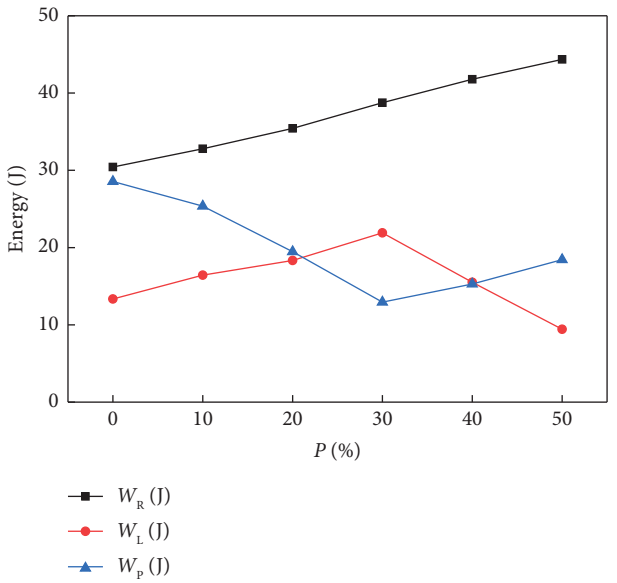

Figure 14: Change curve of each energy of concrete with fly ash content change.

of concrete could be obtained from the energy conservation relationship, as shown in equation (14) [32, 33]:

$$W_L = W_I - W_R - W_P. \tag{13}$$

5.2. Influence on Energy Dissipation Characteristics of Concrete with Fly Ash Contents. By substituting the original waveform into formula (12) and combining with formula (13), the energy of concrete with different fly ash contents could be obtained through calculation. The energy of concrete with different fly ash contents is shown in Table 5.

Figure 14 shows the change curve of each energy of concrete with the fly ash content P. It can be seen in Figure 14 that the reflected energy, transmitted energy, and dissipated energy showed different trends with the change of fly ash content. When the fly ash content increased from 0 to 50%, the reflection energy increased gradually from 30.43 J to 44.36 J with an increase of 45.78%. The dissipation energy increased first and then decreased, and it increased from 13.35 J to 21.91 J with an increase of 64.12% when the fly ash content increased from 0 to 30% but decreased from 21.91 J to 9.43 J with a decrease of 56.96% when the fly ash content increased from 30% to 50%. The transmission energy decreased from 28.56 J to 12.94 J with a decrease of 54.69% when the fly ash content increased from 0 to 30%, while it increased from 12.94 J to 18.44 J with an increase of 42.50% when the fly ash content increased from 30% to 50%. The relationship between the three energies and fly ash content is shown in formula (14).

The change of energy indicated that the amount of fly ash has an important effect on the energy dissipation of concrete. On the one hand, the fly ash, as a kind of industrial slag, contained a large number of spherical particles of minerals. It would have a good filling effect on the pores inside the concrete by mixing these mineral spherical particles in the concrete production process. As a result, the uniformity and compacting of concrete were both improved, and the fly ash also played a good lubrication role in the mixing process, which was conducive to the combination of various substances.

$$\begin{cases} W_R = 0.0005P^2 + 0.2615P + 30.276, & R^2 = 0.9981, \\ W_L = -0.0141P^2 + 0.6571P + 12.469, & R^2 = 0.8741, \\ W_P = 0.0116P^2 - 0.8275P + 30.101, & R^2 = 0.8986. \end{cases} \tag{14}$$

5.3. Calculation Principle of Surface Specific Energy of Fly Ash Concrete. Due to the different fly ash content, the concrete samples would be broken into different particle size fragments under the same air pressure. In order to study the influence of fly ash content change on the surface area of these fragments accurately, the fragments with different particle sizes are transformed into spheres of corresponding size. The number of spheres with the same particle size was calculated according to equation (15) [34]:

$$b_i = \frac{m_i}{\pi r_i^3 \rho / 6}, \tag{15}$$

where b_i is the number of spheres in the particle size range i, m_i is the mass of fragments in the particle size range i, and ρ is the density of fly ash concrete.

By using formula (15) for the number of spheres with different particle sizes, the surface area of fragments could be obtained further. The internal failure area could be obtained by subtracting the upper and lower surface area and side area of the cylinder before broken from the sum of the surface area of all fragments, as shown in equation (16) [34]:

$$S_P = \sum_{i=1}^{8} b_i \pi r_i^2 - 2\pi rh - 2\pi r^2, \tag{16}$$

where r, h were the radius and height of concrete sample before test, respectively.

The work of external forces on concrete caused the concrete to separate from each other and form pieces under impact compression. The internal microcracks developed and then expanded to form a macroscopic fracture surface. It is an energy dissipation process, and the required energy sum is the dissipation energy. Therefore, the relationship between surface specific energy and dissipation energy was [34]

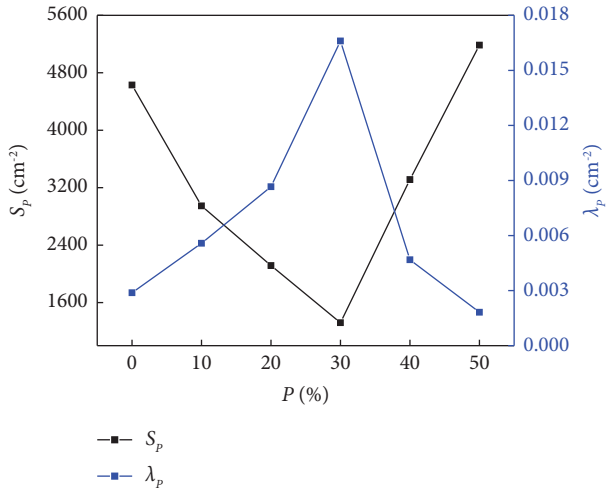

Figure 15: Change curves of surface area and surface specific energy with fly ash content.

$$\mathbf{W_L = S_P \lambda_P}. \tag{17}$$

By using the dissipated energy and the surface area of the fragments, the surface specific energy of the concrete fragments per unit area could be obtained [34]:

$$\boldsymbol{\lambda_P} = \frac{\mathbf{W_L}}{\mathbf{S_P}}. \tag{18}$$

5.4. Influence on Surface Specific Energy of Concrete with Fly Ash Contents. The change law of surface area and surface specific energy of concrete fragments with fly ash content could be calculated by equations (17) and (18) as shown in Figure 15. It could be seen from Figure 15 that the surface area of fragments first decreases and then increases with the increase of fly ash content and reaches the minimum when the fly ash content is 30%. The surface area of concrete fragments is 4630.06 cm^2 when the fly ash content is 0, while it is 1319.65 cm^2 with a decrease of 71.5% when the fly ash content is 30%. With the increase of fly ash content, the surface area of concrete fragments is 5185.49 cm^2 when the fly ash content is 50%, which is 292.95% increase compared with that when the fly ash content is 30%.

The surface specific energy of concrete first increased and then decreased with the increase of fly ash content and reached the maximum when the fly ash content is 30%. The concrete surface specific energy is 0.0029 J·cm^{-2} when the fly ash content is 0, while is 0.0166 J·cm^{-2} with an increase of 475.82% when the fly ash content increases to 30%. With the increase of fly ash content, the concrete surface specific energy is 0.0018 J·cm^{-2} when the fly ash content is 50%, which is 89.05% decrease compared with that when the fly ash content is 30%.

It could be seen from Figure 15 that the fly ash content has an important effect on the surface area of concrete fragments and the specific surface energy of concrete. The internal bonding force of concrete was affected by both fly ash and cement. The cement has a bonding effect. The addition of fly ash filled the internal pores of concrete to a certain extent and played a lubricating role in the concrete production process. At the same time, the secondary hydration reaction also increased the adhesive force of concrete partly. However, the cement content would decrease with the increase of fly ash content with a certain water-cement ratio, leading to the decrease of the bonding force in concrete and the stability of concrete. Based on the joint influence of the two on the performance of concrete, its properties changed with the change of fly ash content under a certain water-cement ratio. Therefore, the surface area of the fragments gradually decreased when the fly ash content of concrete increased from 0 to 30% under the same water-cement ratio and air pressure impact, leading to fewer microcracks and macroscopic broken surfaces due to the combined action of fly ash and cement. The surface area of the fragments gradually increased when the fly ash content of concrete increased from 30% to 50%. Due to the cohesive force of fly ash in concrete is smaller than that of cement, the amount of cement decreased when the amount of fly ash increased. Thus, the bonding force between concrete particles is reduced, and microcracks were more likely to develop and form macroscopic fracture surface under the impact.

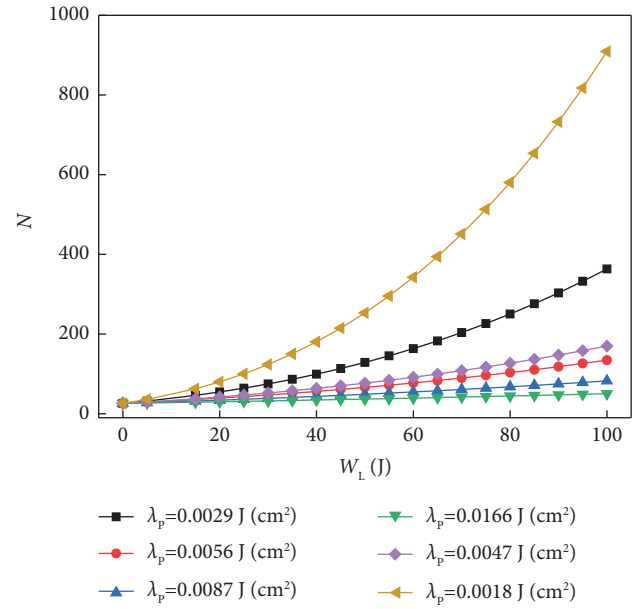

Figure 16: Relationship between concrete breakage degree and dissipative energy with different surface specific energy.

5.5. Application of Fly Ash Concrete in Rock Burst Mines. Fly ash concrete columns could often be used as supporting tools in the rock burst mines. The process of absorptive capacity, energy accumulation, and energy dissipation (without considering the energy loss of heat energy, radiation energy, and kinetic energy) would occur in fly ash concrete under the impact load. The dissipated energy played an important role in the formation of fragments of fly ash concrete. Therefore, all fragments on-site could be simply regarded as spheres of the same size combined with the surface specific energy characteristics when the

proportion of fly ash concrete was known. According to the number of fragments on-site, the dissipation energy was estimated preliminarily, and the calculation formula was as follows [34]:

$$\mathbf{N} = \frac{\left(\mathbf{W_L}/\boldsymbol{\lambda_P} + 2\boldsymbol{\pi}\mathbf{RH} + 2\boldsymbol{\pi}\mathbf{R}^2\right)^3}{36\boldsymbol{\pi}^3\mathbf{R}^4\mathbf{H}^2}, \quad (19)$$

where N was the number of fragments after the equivalent volume, W_L was the dissipated energy, ranging from 0 to 100 J, λ_P was the surface specific energy of fly ash concrete, R was the diameter of underground concrete pillar, with a value of 30 cm, and H was the height of the underground concrete pillar, with a value of 100 cm.

Figure 16 shows the relationship between concrete breakage degree and dissipative energy with different surface specific energy. It can be seen from Figure 16 that the greater the dissipation energy is, the more the number of fragments is formed under different surface specific energy. But the greater the surface specific energy is, the less the number of fragments formed under the same dissipation energy. This is because that the surface specific energy is used as a kind of ability to resist crack formation, and the greater the surface specific energy is, the more difficult for converting the accumulated energy absorbed by concrete into the surface energy for crack propagation is. Therefore, the proportion of concrete used to prevent impact in rock burst mine could be adjusted according to the need, and the amount of dissipated energy could also be estimated on-site preliminarily according to the number of fragments of fly ash concrete.

6. Conclusion

In this article, the impact compression test was carried out with different fly ash contents under 0.3 MPa pressure by using the SHPB systems, and the screening test was carried out on the fragments. The influence of the change of fly ash content on the mechanical characteristics, fragmentation distribution, energy dissipation, and surface specific energy of concrete was explored. The conclusions were as follows:

(1) With the increase of fly ash content, the dynamic peak stress and dynamic residual stress of concrete increased first and then decreased and reached the maximum when the fly ash content was 30%; the dynamic peak strain and dynamic residual strain of concrete decreased first and then increased and reached the maximum when the fly ash content was 30%; the ductility of concrete decreased gradually, that is, it reached the maximum when the ductility of concrete was without fly ash.

(2) With the increase of fly ash content, the particle size of concrete first increased and then decreased and reached the maximum when the fly ash content was 30%; the fractal dimension of concrete decreased first and then increased and reached the minimum when the fly ash content was 30%.

(3) With the increase of fly ash content, the reflected energy increased gradually, the transmitted energy decreased first and then increased, and it reached the minimum when the fly ash content was 30%, while the dissipated energy increased first and then decreased and reached the maximum when the fly ash content was 30%.

(4) With the increase of fly ash content, the surface area of the fragments decreased first and then increased and reached the minimum when the fly ash content was 30%, while the surface specific energy of concrete increased first and then decreased and reached the maximum when the fly ash content was 30%. The greater the dissipated energy was, the more pieces were formed under different surface specific energy, while the greater the surface specific energy was, the less pieces were formed under the same dissipation energy.

Data Availability

The data of the pictures and tables used to support the findings of this study are included within the article.

Conflicts of Interest

The author declares no conflicts of interest regarding the publication of this paper.

Authors' Contributions

All authors have read and agreed to the published version of the manuscript.

Acknowledgments

This work was supported by the National Natural Science Foundation of China (grant numbers 52174175 and 51774110), Program for Science and Technology Innovation Talents in Universities of Henan Province (grant number 19HASTIT047), and Science and Technology Project of Henan Province (grant number 222102320096).

References

[1] S. Akdag, M. Karakus, G. D. Nguyen, A. Taheri, and T. Bruning, "Evaluation of the propensity of strain burst in brittle granite based on post-peak energy analysis," *Underground Space*, vol. 6, no. 1, pp. 1–11, 2021.

[2] C. Mark and M. Gauna, "Pillar design and coal burst experience in utah book cliffs longwall operations," *International Journal of Mining Science and Technology*, vol. 31, no. 1, pp. 33–41, 2021.

[3] B. Sun, Y. Ping, and Z. Zhu, "Experimental study on the dynamic mechanical properties of large-diameter mortar and concrete subjected to cyclic impact," *Shock and Vibration*, vol. 2020, Article ID 8861197, 9 pages, 2020.

[4] B. Cantero, M. Bravo, J. de Brito, I. F. S. del Bosque, and C. Medina, "The influence of fly ash on the mechanical performance of cementitious materials produced with recycled cement," *Applied Sciences*, vol. 12, no. 4, p. 2257, 2022.

[5] M. F. M. Tahir, M. M. A. B. Abdullah, S. Z. A. Rahim et al., "Mechanical and durability analysis of fly ash based

geopolymer with various compositions for rigid pavement applications," *Materials*, vol. 15, no. 10, p. 3458, 2022.

[6] F. Koksal, O. Gencel, Y. Sahin, and O Okur, "Recycling bottom ash in production of eco-friendly interlocking concrete paving blocks," *Journal of Material Cycles and Waste Management*, vol. 23, no. 3, pp. 985–1001, 2021.

[7] S. R. Da Silva and J. J. Andrade, "A review on the effect of mechanical properties and durability of concrete with construction and demolition waste (CDW) and fly ash in the production of new cement concrete," *Sustainability*, vol. 14, no. 11, p. 6740, 2022.

[8] S. R. Da Silva and D. O. A. J. Jose, "Investigation of mechanical properties and carbonation of concretes with construction and demolition waste and fly ash," *Construction and Building Materials*, vol. 153, no. 30, pp. 704–715, 2017.

[9] S. V. Vassilev, R. Menendez, D. Alvarez, M. Diaz-Somoano, and M. Martinez-Tarazona, "Phase-mineral and chemical composition of coal fly ashes as a basis for their multicomponent utilization. 1. Characterization of feed coals and fly ashes☆," *Fuel*, vol. 82, no. 14, pp. 1793–1811, 2003.

[10] S. Wang, E. Llamazos, L. Baxter, and F. Fonseca, "Durability of biomass fly ash concrete: f," *Fuel*, vol. 87, no. 3, pp. 359–364, 2008.

[11] S. Rukzon and P. Chindaprasirt, "Strength and chloride resistance of blended Portland cement mortar containing palm oil fuel ash and fly ash," *International Journal of Minerals, Metallurgy and Materials*, vol. 16, no. 4, pp. 475–481, 2009.

[12] F. U. A. Shaikh, "Mechanical and durability properties of fly ash geopolymer concrete containing recycled coarse aggregates," *International Journal of Sustainable Built Environment*, vol. 5, no. 2, pp. 277–287, 2016.

[13] S. Nasir, "Comparison of engineering and durability properties of fly ash blended cement concrete made in uk and malaysia," *Advances In Applied Ceramics*, vol. 106, no. 6, pp. 314–318, 2007.

[14] B. Brueggen, T. H. K. Kang, and C. Ramseyer, "Experimental and SEM analyses of ground fly ash in concrete," *International Journal of Concrete Structures and Materials*, vol. 4, no. 1, pp. 51–54, 2010.

[15] P. Chindaprasirt, C. Chotithanorm, H. T. Cao, and V. Sirivivatnanon, "Influence of fly ash fineness on the chloride penetration of concrete," *Construction and Building Materials*, vol. 21, no. 2, pp. 356–361, 2007.

[16] T. Simčič, S. Pejovnik, G. De Schutter, and V. B. Bosiljkov, "Chloride ion penetration into fly ash modified concrete during wetting–drying cycles," *Construction and Building Materials*, vol. 93, pp. 1216–1223, 2015.

[17] N. Bouzoubaa, M. H. Zhang, and V. M. Malhotra, "Laboratory-producedhigh-volume fly ash blended cements: compressive strength and resistance to the chloride-ion penetration of concrete," *Cement and Concrete Research*, vol. 30, no. 7, pp. 1037–1046, 2000.

[18] W. M. Zhang, S. F. Chen, and H. J. Ba, "Research on deformation performance of fly ash concrete under repeated stress," *Advances in Structural Engineering*, vol. 2, 2006.

[19] M. H. Mussa, A. M. Abdulhadi, I. S. Abbood, A. A. Mutalib, and Z. M. Yaseen, "Late age dynamic strength of high-volume fly ash concrete with nano-silica and polypropylene fibres," *Crystals*, vol. 10, no. 4, p. 243, 2020.

[20] Y. Wang, H. Zhong, and M. Zhang, "Experimental study on static and dynamic properties of fly ash-slag based strain hardening geopolymer composites," *Cement and Concrete Composites*, vol. 129, Article ID 104481, 2022.

[21] B. Szostak and G. L. Golewski, "Rheology of cement pastes with siliceous fly ash and the CSH nano-admixture," *Materials*, vol. 14, no. 13, p. 3640, 2021.

[22] K. Khan, A. Ahmad, M. N. Amin, W. Ahmad, S. Nazar, and A. M. A. Arab, "Comparative study of experimental and modeling of fly ash-based concrete," *Materials*, vol. 15, no. 11, p. 3762, 2022.

[23] K. Liu, R. Song, J. Li et al., "Effect of steel fiber type and content on the dynamic tensile properties of ultra-high performance cementitious composites (UHPCC)," *Construction and Building Materials*, vol. 342, Article ID 127908, 2022.

[24] H. Zhang, L. Bai, Y. Qi, H. Hong, A. Neupane, and Q. Pan, "Impact of splitting tensile properties and dynamic constitutive model of fly ash concrete," *Journal of Materials in Civil Engineering*, vol. 32, no. 8, Article ID 04020225, 2020.

[25] Z. Tang, W. Li, V. W. Y. Tam, and Z. Luo, "Investigation on dynamic mechanical properties of fly ash/slag-based geopolymeric recycled aggregate concrete," *Composites Part B: Engineering*, vol. 185, Article ID 107776, 2020.

[26] J. Xie, J. Zhao, J. Wang, C. Fang, B. Yuan, and Y. Wu, "Impact behaviour of fly ash and slag-based geopolymeric concrete: the effects of recycled aggregate content, water-binder ratio and curing age," *Construction and Building Materials*, vol. 331, Article ID 127359, 2022.

[27] X. S. Shi, F. G. Collins, X. L. Zhao, and Q. Wang, "Mechanical properties and microstructure analysis of fly ash geopolymeric recycled concrete," *Journal of Hazardous Materials*, vol. 238, pp. 20–29, 2012.

[28] H. Zhou, F. Meng, and C. Zhang, "Quantitative evaluation of rock brittleness based on stress-strain curve," *Chinese Journal of Rock Mechanics and Engineering*, vol. 33, no. 6, pp. 1114–1122, 2014.

[29] L. Ming, *Research on Rupture Mechanisms of Coal Measures Sandstone under High Temperature and Impact Load*, China University of Mining and Technology, Xuzhou, China, 2014.

[30] B. Li, *Research on Creep Properties and Damage Rupture Mechanism of Concrete under Freeze-Thaw Effect*, China University of Mining and Technology, Xuzhou, China, 2016.

[31] P. Wu, L. Zhang, and X. Mao, "Coupling effect of strain rate and freeze-thaw temperature on dynamic mechanical properties and fractal characteristic of saturated yellow sandstone," *Geofluids*, vol. 2021, Article ID 7511467, 14 pages, 2021.

[32] M. Li, X. Mao, L. Cao, H. Pu, R. Mao, and A. Lu, "Effects of thermal treatment on the dynamic mechanical properties of coal measures sandstone," *Rock Mechanics and Rock Engineering*, vol. 49, no. 9, pp. 3525–3539, 2016.

[33] M. Li, X. Mao, L. Cao, H. Pu, and A. Lu, "Influence of heating rate on the dynamic mechanical performance of coal measure rocks," *International Journal of Geomechanics*, vol. 17, no. 8, Article ID 04017020, 2017.

[34] Z. Z. Zhang, "Energy evolution mechanism during rock deformation and failure," China University of Mining and Technology, Xuzhou, China, 2016.